JOURNAL OF AIRCRAFT
Vol. 34, No. 1, January–February 1997

High-Lift Low Reynolds Number Airfoil Design

Michael S. Selig* and James J. Guglielmo†
University of Illinois at Urbana–Champaign, Urbana, Illinois 61801

A new high-lift airfoil design philosophy has been developed and experimentally validated through wind-tunnel tests. A key element of the high-lift design philosophy was to make use of a concave pressure recovery with aft loading. Three codes for airfoil design and analysis (PROFOIL, the Eppler code, and ISES) were used to design the example S1223 high-lift airfoil for a Reynolds number of 2×10^5. In wind-tunnel tests, the new airfoil yielded a maximum lift coefficient of 2.2. With vortex generators and a 1% chord Gurney flap (used separately), the $C_{l,\max}$ increased to 2.3. The airfoil demonstrates the rather dramatic gains in $C_{l,\max}$ over those airfoils previously used for high-lift low Reynolds number applications.

Nomenclature

C_d = airfoil drag coefficient
C_l = airfoil lift coefficient
$C_{l,\max}$ = airfoil maximum lift coefficient
$C_{m,c/4}$ = airfoil pitching-moment coefficient about the quarter-chord point
c = airfoil chord
V = velocity distribution nondimensionalized by the freestream
x = airfoil x coordinate
α = angle of attack relative to chord line

I. Introduction

INCREASED payloads, shortened takeoff and landing distances, reduced aircraft noise, and lowered stall speeds can all be derived from the beneficial effects of improved high-lift airfoil aerodynamics. It is, therefore, not surprising that the classic problem of high-lift airfoil design has been and remains a topic of considerable interest.[1–4] The purpose of this paper is to present a high-lift airfoil design philosophy for the increasingly important low Reynolds number regime in which small unmanned aerial vehicles (UAVs) operate. Only single-element airfoils are considered in the current work.

Airfoils for such aircraft typically operate in the Reynolds number range 2×10^5 to 5×10^5. For example, U.S. Navy electronic warfare UAVs (e.g., LAURA[5] and FLYRT[6,7] aircraft) fly at ship-like speeds ranging from 25 to 40 kn with payload requirements varying from 10 to 25 lb. The small vehicle size required for efficient shipboard storage coupled with low flight speeds and demanding payload requirements places great emphasis on high-lift low Reynolds number aerodynamics. A similar-sized aircraft, the hand-launched Pointer UAV operated by the U.S. Army,[8] is used to perform short-range reconnaissance missions. Moreover, small payload-laden UAVs have been envisioned for missions that involve atmospheric sampling, border surveillance, forest fire detection/tracking, ship- or aircraft-wreck survivor search and weather monitoring. In each case, high-lift airfoil performance can to varying degrees play an important role.

To place the current work in a proper global context, Fig. 1 presents the maximum lift characteristics of a number of representative low-speed airfoils taken from various sources.[1,9–16] Although not all of these airfoils were specifically designed for high-lift, a predictable and anticipated trend emerges, the lower the Reynolds number, the lower the maximum lift. In particular, in going from a Reynolds number of 1×10^6 to 1×10^5, a sharp drop in $C_{l,\max}$ is seen in the available data. The lower end of this range is of interest in the design of small UAVs based on current trends.[6] In particular, this paper focuses on high-lift airfoil design for a Reynolds number of 2×10^5.

High lift is rarely the only desirable feature of an airfoil. The airfoil lift-to-drag ratio, endurance parameter, thickness, pitching moment, stall characteristics, and sensitivity to roughness are all important factors, among others, that must each be weighed separately when one considers selecting or designing an airfoil. This study focuses on those factors most related to enhanced high-lift low Reynolds numbers airfoil performance.

II. Experiments

This section describes the wind-tunnel experiment used to validate the design philosophy discussed in the next section.

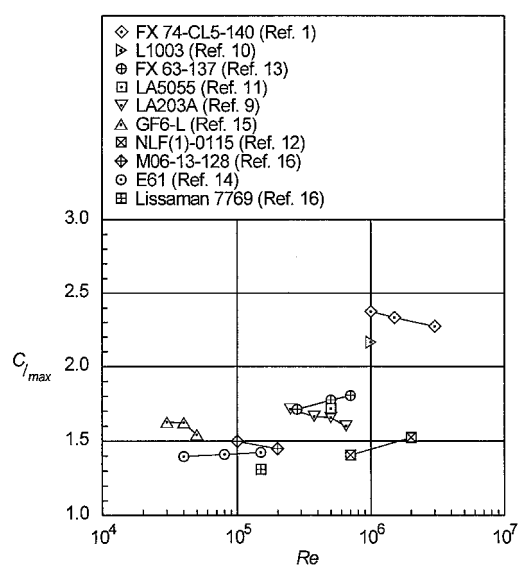

Fig. 1 Maximum lift coefficient of several airfoils over a range of Reynolds numbers.

Presented as Paper 94-1866 at the AIAA 12th Applied Aerodynamics Conference, Colorado Springs, CO, June 20–23, 1994; received Nov. 25, 1995; revision received Oct. 15, 1996; accepted for publication Oct. 26, 1996.

*Assistant Professor, Department of Aeronautical and Astronautical Engineering, 306 Talbot Laboratory, 104 South Wright Street. Member AIAA.

†Graduate Research Assistant, Department of Aeronautical and Astronautical Engineering; currently Engineer/Scientist, McDonnell Douglas Aerospace, Advanced Systems and Technology/Phantom Works, Mail Code 71-35, 2401 East Wardlow Road, Long Beach, CA 90807-5309. Member AIAA.

Since details of the method can be found in Refs. 17–21, only a summary is given here.

A. Wind-Tunnel and Measurement Techniques

The experiments were performed in the University of Illinois open-return subsonic wind tunnel. The rectangular test-section dimensions are approximately 2.8 × 4 ft in cross section and 8 ft long. To ensure good flow quality in the test section, the tunnel settling chamber contains a 4 in.-thick honeycomb and four antiturbulence screens, resulting in a turbulence level of less than 0.1% over the Reynolds number range tested.

The experimental setup is shown in Fig. 2. To isolate the ends of the airfoil model from the tunnel side-wall boundary layers and the outer support hardware, the airfoil models were mounted horizontally between two $\frac{3}{8}$ in.-thick, 6 ft-long Plexiglas® splitter plates (not shown in Fig. 2 for clarity). Gaps between the model and splitter plates were nominally 0.05 in. All models had a 12-in. chord and $33\frac{5}{8}$-in. span. One side of the model was free to pivot (far side of Fig. 2). At this location, the angle of attack was measured using an ac potentiometer (rotary transformer). The other side of the model was free to move vertically on a precision ground shaft, but not free to rotate. A servo-feedback-control force balance, however, restrained the motion of the model and measured the lift force. Linear and spherical ball bearings within the lift carriage helped to minimize any frictional effects.

The drag was obtained from the momentum method. To ensure that the wake had relaxed to tunnel static pressure, the wake measurements were performed 14.8 in. (approximately 1.25-chord lengths) downstream of the model trailing edge. Each vertical wake traverse consisted of between 20–80 total-head pressure measurements (depending on wake thickness) with points nominally spaced 0.08 in. apart. Owing to spanwise wake nonuniformities,[17,18] wake profile measurements were taken at four spanwise locations spaced 4 in. apart over the center 12 in. of the model span. The resulting four drag coefficients were then averaged to obtain the drag at a given angle of attack.

The lift, drag, and angle-of-attack measurements were corrected to account for the effects of solid blockage, wake blockage, and streamline curvature.[22] The velocity was not only corrected for solid and wake blockage but also for a circulation effect that is unique to setups that make use of splitter plates. For the current tests, the freestream velocity, rather than being measured far upstream, had to be measured between the splitter plates because of a spillage effect (air flowing between the splitter plates and the tunnel side-walls). Since the pitot-static probe that was used to measure the freestream was located fairly close to the model, the probe measurements were therefore corrected for airfoil circulation effects so as to obtain the true freestream test section speed. The details of this correction procedure can be found in Ref. 21.

Overall uncertainty in the lift coefficient is estimated to be 1.5%. The drag measurement error comes from three sources: 1) accuracy of the data acquisition instruments, 2) repeatability of the measurements, and 3) the locations of the particular four wake profiles used to determine the average drag coefficient. Based partly on the error analysis method presented in McGhee et al.[23] and Coleman and Steele,[24] the uncertainty caused by the instruments and measurement repeatability are less than 1 and 1.5%, respectively. Based on a statistical analysis (for a 95% confidence interval) of the spanwise drag results for the E374 airfoil[17] at $\alpha = 4$ deg, the uncertainties caused by the spanwise variations were estimated to be 3% for $Re = 1 \times 10^5$ and reduce to approximately 1.5% at and above $Re = 2 \times 10^5$. The current airfoils are expected to have approximately the same uncertainties. A more detailed discussion of this topic is presented in Ref. 18. For the angle-of-attack sensor, the uncertainty is estimated to be 0.08 deg.

B. Model Accuracy

To determine the accuracy of airfoil profiles, each model was digitized with a Brown & Sharpe coordinate measuring machine. Approximately 80 points were taken around each airfoil, and the spacing between points was approximately pro-

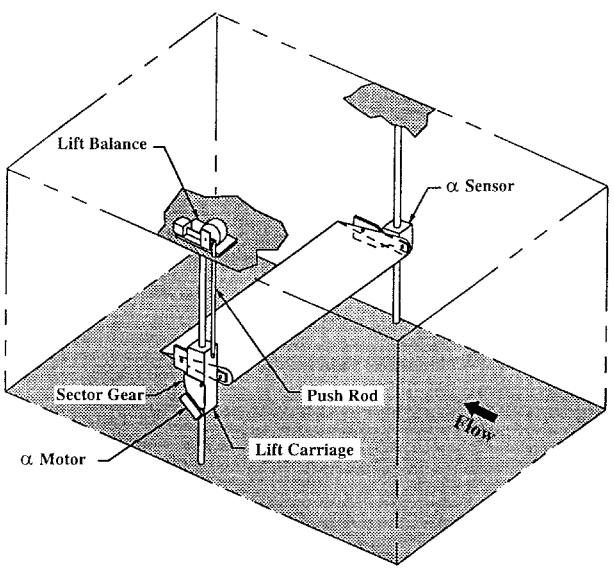

Fig. 2 Wind-tunnel test section with model installed (splitter plates and traverser omitted for clarity).

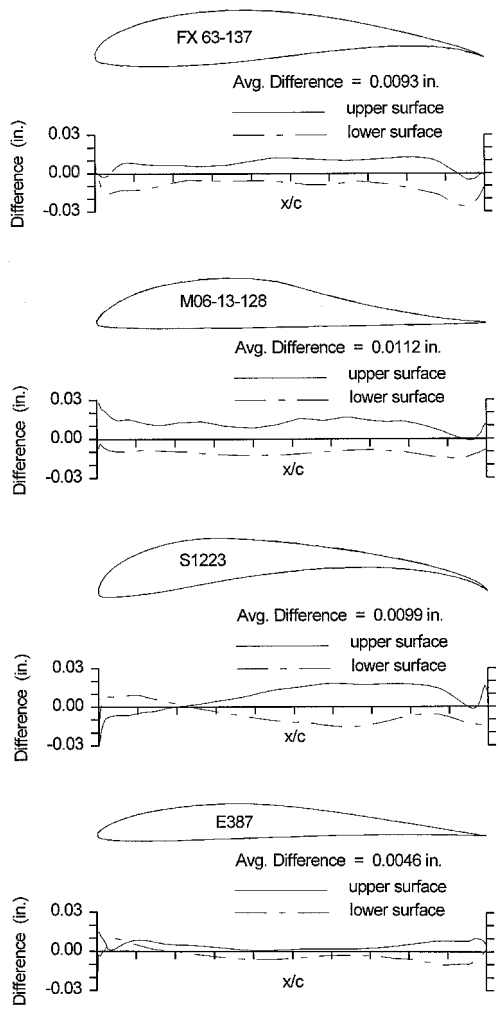

Fig. 3 Comparison between measured model coordinates and true coordinates.

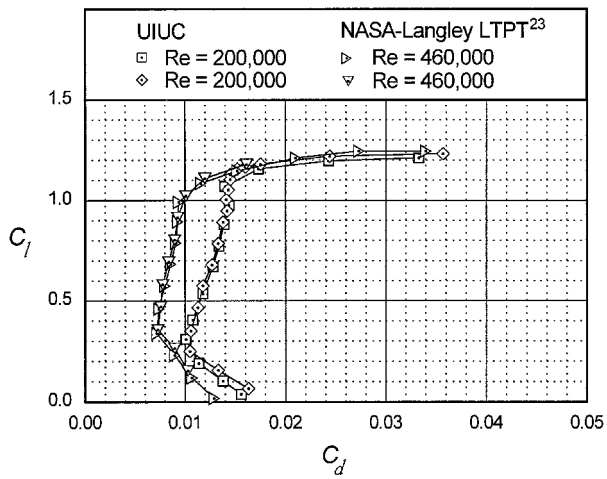

Fig. 4 Comparison of the E387 measured drag polars.

portional to the local curvature. Thus, near the leading and trailing edges, the spacing was relatively small, whereas over the midchord it was no greater than 0.7 in. These measured coordinates were compared with the true coordinates using a two-dimensional least-squares approach (rotation and vertical translation), which yielded an average difference of approximately 0.010 in. for all airfoils discussed in this paper. Figure 3 shows a comparison of the FX 63-137 measured model coordinates (dot–dash line) and true coordinates (solid line). Also shown are the M06-13-128, S1223, and E387 airfoils for later reference. Each plot depicts the differences between the model airfoil and the true coordinates for the airfoil upper surface (solid line) and lower surface (dot–dash line). A displacement above or below the axis means that the model surface lies above or below the true coordinates, respectively. For instance, the FX 63-137 model was thicker than the true coordinates by approximately 0.009 in. over most of the airfoil chord.

C. Validation

Data taken on the E387 model for $Re = 2 \times 10^5$ and 4.6×10^5 are shown in Fig. 4 and compared with data taken in the NASA Langley Research Center's Low-Turbulence Pressure Tunnel (LTPT).[23] As seen, good agreement is observed, and this serves to validate the current experiments. Moreover, surface oil-flow visualization taken to determine the laminar separation and oil-accumulation lines showed that the lines agreed with NASA Langley Research Center's LTPT data to within 1–2% of chord.[25] (It should be noted that a previous version of the E387[17,18] was less accurate than the current model, and this led to discrepancies when compared with the LTPT data. It should also be noted that data shown previously,[17] from Delft[26] and Stuttgart,[14] was obtained from only one wake profile measurement and is therefore subject to error, because, as mentioned earlier, the wake profiles should be taken at several spanwise stations and averaged.[17,18])

III. Design Philosophy

The high-lift low Reynolds number airfoil design philosophy to be discussed can be illustrated by considering the Wortmann FX 63-137[13] and Miley M06-13-128[3] airfoils. The inviscid velocity distribution for the FX 63-137 (for $C_l = 1.5$) as well as the measured drag polar and lift characteristics are shown in Figs. 5–7, respectively. For reference, a $C_l = 1.5$ for the FX 63-137 corresponds to a value approximately 10% less than the viscous $C_{l,\max}$. Data for the M06-13-128 are shown in Figs. 8–10. The inviscid velocity distribution in this case corresponds to $C_l = 1.35$, again approximately 10% less than the viscous $C_{l,\max}$. No special significance should be given to these C_l values, except that they are close to the respective $C_{l,\max}$ values. Although the viscous velocity distributions differ from the inviscid ones owing to laminar separation bubble effects, much can be gleaned nonetheless from the inviscid velocity distributions. The experimental data was taken in the UIUC subsonic wind tunnel as described in the previous section. For the lift curves, the solid-triangle and open-circle symbols are for increasing and decreasing angles of attack, respectively.

Figure 11 shows the pitching moment characteristics vs the type of upper-surface pressure recovery for several airfoils, including not only the FX 63-137 and M06-13-128, but also

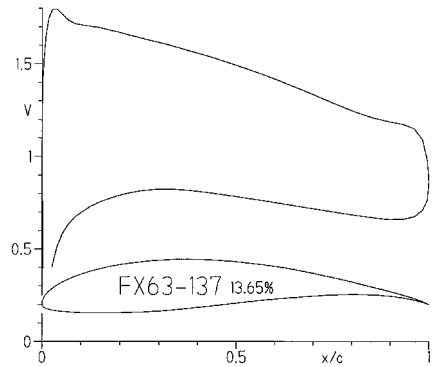

Fig. 5 Inviscid velocity distribution for the FX 63-137 airfoil at $C_l = 1.5$.

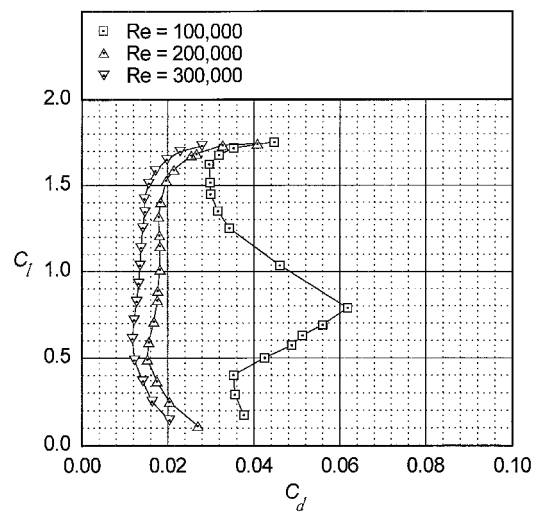

Fig. 6 Drag polar for the FX 63-137 airfoil.

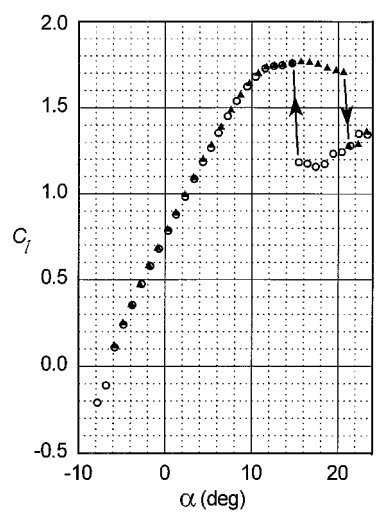

Fig. 7 Lift characteristics for the FX 63-137 airfoil at $Re = 2 \times 10^5$.

others that could be used to equally illustrate the design philosophy. Some of the information used to construct the figure is presented in Table 1. The FX 63-137 with its relatively high (negative) pitching moment and convex pressure recovery appears toward the upper left corner. In contrast, airfoils with a Stratford-like concave pressure recoveries and low pitching moments, such as the Miley M06-13-128 airfoil, appear on the lower right. Also shown in Fig. 11 are several trend lines that, together with the moment and recovery-type information, can be used to deduce a strategy for high-lift low Reynolds number airfoil design. It should be noted that the figure is used to only illustrate the trends and qualitative ideas discussed. Thus, it is not intended to be wholly accurate with respect to the placement of the airfoils. For instance, two airfoils can have the same pitching moment and similar recovery distributions, and hence, occupy the same point on the plot, yet these two airfoils could exhibit different camber $C_{l,\max}$, and stall characteristics. In the figure, the airfoils are placed most accurately with respect to the $C_{l,\max}$ and shape of the recovery distribution.

One trend depicted in Fig. 11 is that an airfoil typically becomes more cambered when the pitching moment increases and/or when the recovery becomes less concave and more convex. Another trend is that the trailing-edge stall becomes more abrupt as the pressure recovery becomes less convex and more concave. Stall rate (as denoted in Fig. 11) refers to the shape of the lift curve at stall. The FX 63-137 is an example of an airfoil with a slow trailing-edge stall for which the point of turbulent separation slowly progresses forward as the angle of attack increases. As shown in Fig. 7, the plateau in the lift curve past the point of stall initiation is indicative of the slow movement of the separation point. The M06-13-128 (Fig. 10) is an example of an airfoil that has a moderate trailing-edge stall. The lift curve peaks at $C_{l,\max}$, then falls off more rapidly than the FX 63-137 airfoil. This characteristic is indicative of a turbulent separation point that moves forward more quickly with increasing angle of attack.

The last trend shown in Fig. 11 is that the maximum lift coefficient increases as the pitching moment increases and as the pressure recovery approaches that of a Stratford distribution. The FX 63-137 is a good example of increasing the $C_{l,\max}$ primarily through added pitching moment. In contrast, classic Liebeck-type airfoils[10] (such as the M06-13-128) are good examples of increasing the $C_{l,\max}$ mainly through the use of a Stratford distribution.

Specifically, the Liebeck high-lift design philosophy[10] involves using a Stratford distribution to recover the most pressure without separation at $C_{l,\max}$. Since separation is avoided entirely, the prototypical Liebeck airfoil is one with no aft loading, which yields a low pitching moment. The M06-13-128 serves as an example of applying the Liebeck design phi-

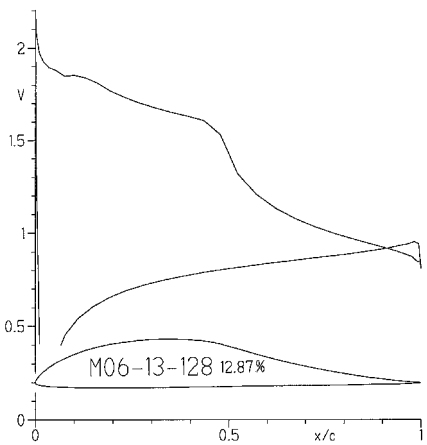

Fig. 8 Inviscid velocity distribution for the M06-13-128 airfoil at C_l = 1.35.

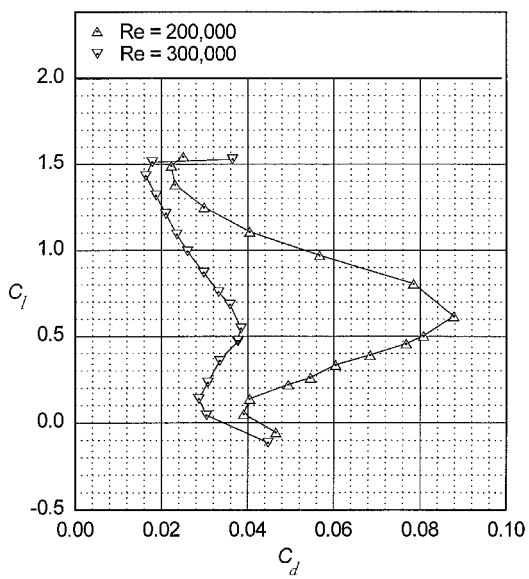

Fig. 9 Drag polar for the M06-13-128 airfoil.

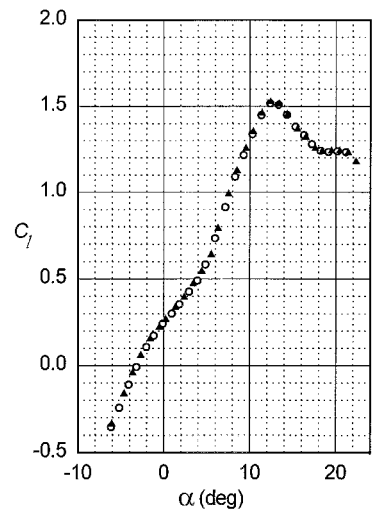

Fig. 10 Lift characteristics for the M06-13-128 airfoil at Re = 2 × 10^5.

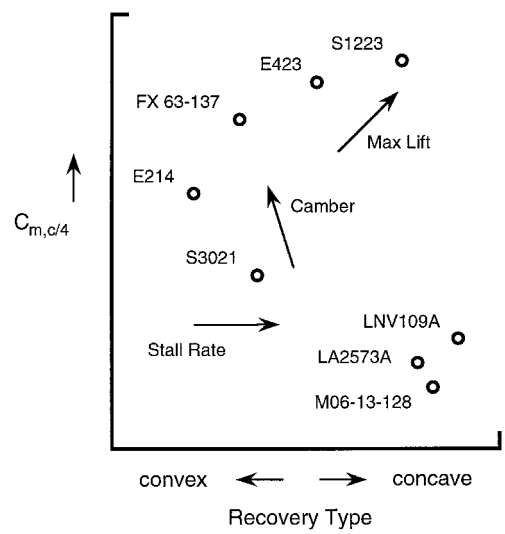

Fig. 11 Trends in low Reynolds number airfoil characteristics as functions of the pitching moment and type of upper-surface pressure recovery distribution.

Table 1 Tabulated data for airfoils in Fig. 11

Airfoil	$C_{l,\max}$	$C_{m,c/4}$	Re	Reference
E214	1.25	−0.11	2×10^5	27
E423	2.00	−0.25[a]	2×10^5	20
FX 63-137	1.75	−0.17[a]	2×10^5	Present paper
M06-13-128	1.52	0.00[a]	2×10^5	Present paper
LA2573A	1.86	0.02	2.5×10^5	9
LNV109A	1.87	−0.02	2.5×10^5	9
S1223	2.23	−0.29[a]	2×10^5	Present paper
S3021	1.17	−0.07	2×10^5	27

[a]Based on predictions.[19,28]

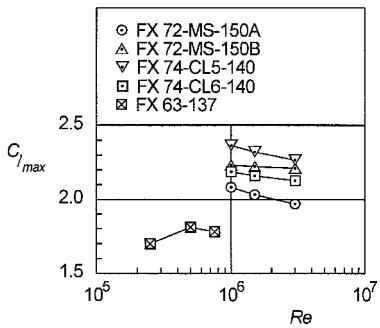

Fig. 12 $C_{l,\max}$ characteristics for five Wortmann airfoils (adapted from Ref. 1).

losophy at low Reynolds numbers. Although the M06-13-128 has a high midrange bubble drag at the off-design Reynolds numbers of 3×10^5, the $C_{l,\max}$ is approximately 1.5. This value for $C_{l,\max}$ is high, especially in light of the intrinsic low pitching moment.

It is argued by Eppler[4] that to achieve maximum lift on an airfoil with a concave Stratford-like recovery, the low pitching-moment constraint should be relaxed. In a computational study for Reynolds numbers above 1×10^6, Eppler[4] showed that the lift of an airfoil with a concave recovery can be increased through the use of aft loading. The airfoils incorporated the favorable effects of both a concave recovery distribution and added pitching moment to achieve high $C_{l,\max}$ values. In Fig. 11, airfoils of this type would appear between the FX 63-137 and M06-13-128, but displaced in the direction of increased lift.

The high-lift design philosophy described by Eppler[4] was employed nearly two decades earlier by Wortmann[1] in the design of the FX 74-CL5-140 airfoil and three more conservative derivative airfoils. Figure 12 shows the $C_{l,\max}$ characteristics of the FX 74-CL5-140 that achieves a $C_{l,\max}$ of nearly 2.4 at a Reynolds number of 1×10^6, as contrasted with the FX 63-137 that only achieves a $C_{l,\max}$ of 1.7–1.8 for the Reynolds number range 2.5×10^5 to 7×10^5. The trend of slightly increasing $C_{l,\max}$ with decreasing Reynolds number has been observed elsewhere[9] and is characteristic of some airfoils at low Reynolds numbers.[19] At first glance, Fig. 1 appears to indicate a general trend that $C_{l,\max}$ for a range of airfoils dramatically decreases with Reynolds number, particularly over the range of interest in this study, namely for $Re = 2 \times 10^5$. Inspection of the FX 74-CL5-140 reveals, however, that it employs a concave recovery[1] as opposed to the convex recovery of the FX 63-137. Thus, in light of the preceding discussion, the main difference in the maximum lift is not because of a Reynolds number effect as suggested by Fig. 12. Rather, the difference is because of the shape of the recovery distribution: convex vs concave.

Since the FX 63-137 is not similar in its design to the FX CL/MS-class airfoil, there appears to be an area of design space that has yet to be explored. Airfoils that would fit into this design space could be considered relatives of the FX CL/MS-class airfoils. It is within this region that an airfoil has been designed with its high-lift characteristics achieved through the use of both a concave recovery and aft loading, two features that have not been previously incorporated into a high-lift airfoil specifically designed for low Reynolds numbers.

IV. Design Methodology

A high-lift airfoil based on the preceding discussion and presented in the following section was designed through the use of several low-speed airfoil design and analysis codes: PROFOIL,[29–31] the Eppler code,[4,32] and ISES.[33] First, PROFOIL was used for rapid interactive design. A new airfoil that appeared to meet the performance objectives was then screened through two more computationally intensive analysis codes, first the Eppler code and then the ISES code. If at any

Table 2 S1223 airfoil coordinates

Upper surface		Lower surface	
x/c	y/c	x/c	y/c
0.00010	0.00286	0.00005	−0.00138
0.00030	0.00745	0.00083	−0.00593
0.00221	0.01365	0.00139	−0.00690
0.00482	0.02100	0.00312	−0.00872
0.00706	0.02587	0.00790	−0.01068
0.01082	0.03257	0.01449	−0.01150
0.01503	0.03884	0.02138	−0.01185
0.01989	0.04487	0.03330	−0.01196
0.02846	0.05369	0.04627	−0.01153
0.03568	0.05999	0.06389	−0.01040
0.04897	0.07000	0.08117	−0.00888
0.06800	0.08199	0.10354	−0.00663
0.08018	0.08863	0.12948	−0.00369
0.09550	0.09613	0.16404	0.00134
0.11009	0.10247	0.20100	0.00781
0.12497	0.10819	0.25115	0.01690
0.14032	0.11348	0.29610	0.02479
0.15733	0.11868	0.33392	0.03100
0.17473	0.12336	0.38160	0.03816
0.19561	0.12802	0.43006	0.04455
0.21283	0.13114	0.47940	0.05004
0.23263	0.13393	0.52654	0.05432
0.26356	0.13679	0.57684	0.05747
0.29648	0.13794	0.63172	0.05939
0.32854	0.13771	0.67649	0.05980
0.35962	0.13665	0.71559	0.05921
0.38752	0.13509	0.73675	0.05844
0.41610	0.13304	0.76333	0.05703
0.44641	0.13039	0.78942	0.05506
0.47863	0.12718	0.80947	0.05310
0.50578	0.12419	0.83028	0.05062
0.53542	0.12074	0.86994	0.04446
0.56407	0.11720	0.89924	0.03838
0.59071	0.11368	0.92149	0.03274
0.61072	0.11087	0.94479	0.02561
0.65038	0.10483	0.95707	0.02117
0.68153	0.09976	0.97177	0.01493
0.71868	0.09328	0.98900	0.00570
0.74802	0.08779	0.99231	0.00363
0.78334	0.08061	0.99800	−0.00013
0.81744	0.07305	1.00000	0.00000
0.84496	0.06638		
0.87178	0.05924		
0.88969	0.05399		
0.91053	0.04728		
0.92548	0.04204		
0.94176	0.03581		
0.95370	0.03080		
0.96293	0.02660		
0.97339	0.02127		
0.98075	0.01692		
0.98689	0.01260		
0.99187	0.00839		
0.99720	0.00333		
1.00000	0.00000		

point the candidate airfoil failed to meet the design goals, the experience gained was used to redesign the airfoil to more closely match the desired high-lift performance objectives. This iterative process continued until a successful airfoil was designed, and subsequently, wind-tunnel tested to validate the design philosophy.

V. Application

The example airfoil presented, the S1223 with coordinates given in Table 2, was designed to achieve a $C_{l,\max}$ greater than 2 for a Reynolds number of 2×10^5. Figure 13 depicts the inviscid velocity distributions for the S1223 for $C_l = 1.95$. Through the use of PROFOIL, the upper-surface velocity distribution corresponding to the design $C_{l,\max}$ was determined from a specified boundary-layer development. In particular, from the leading edge to near $0.20c$, the boundary layer was prescribed to be near laminar separation, an approach that could be considered as a laminar analogy to the turbulent Stratford pressure recovery.[34,35] At $0.20c$, a short bubble ramp was employed. The main pressure recovery was prescribed by specifying the turbulent boundary layer to be increasingly near turbulent separation toward the trailing edge. Finally, aft loading was employed at the trailing edge since, as discussed, the penalty caused by limited trailing-edge separation is expected to be more than offset by the gain in $C_{l,\max}$.

A wind-tunnel model of the S1223 was constructed and tested in the University of Illinois at Urbana–Champaign (UIUC) subsonic wind tunnel. Lift characteristics for a Reynolds number of 2×10^5 are shown in Fig. 14. The results indicate a $C_{l,\max}$ of approximately 2.2, which clearly validates the aforementioned design philosophy. As compared with the $C_{l,\max}$ of 1.75 for the FX 63-137, a $C_{l,\max}$ of 2.2 for the S1223 represents a 25% increase. Thus, again, the FX 63-137 should not be viewed as a high-lift airfoil in a class similar to the FX 74-CL5-140, and the trend lines for $C_{l,\max}$ vs Re indicated in Figs. 1 and 12 are in the current light misleading. The S1223 exhibits acceptable moderate stall characteristics much like the M06-13-128. This characteristic is important for some UAVs that operate with the airfoil near $C_{l,\max}$ to achieve low-speed flight requirements for loiter, cruise, or landing.

In an effort to increase the $C_{l,\max}$ of the S1223, it was tested with vortex generators (VGs) located on the upper surface at $0.17c$ and, separately, with a $0.01c$ Gurney flap as depicted in Fig. 15. As shown in Fig. 16, the VGs produced a $C_{l,\max}$ of 2.3 for increasing angles of attack followed by an abrupt stall and a hysteresis loop between 16–20 deg. Thus, the VGs as tested were not beneficial. The lift performance with the Gurney flap is shown in Fig. 17. As seen, $C_{l,\max}$ is 2.3 with the Gurney flap, and the stall is much like that of the clean airfoil. Unfortunately, lift measurements were only taken for increasing angles of attack, in which case it is not possible to detect hysteresis or lack thereof.

Drag data were taken on the S1223 and shown in Fig. 18. When the drag coefficient exceeded approximately 0.05, no

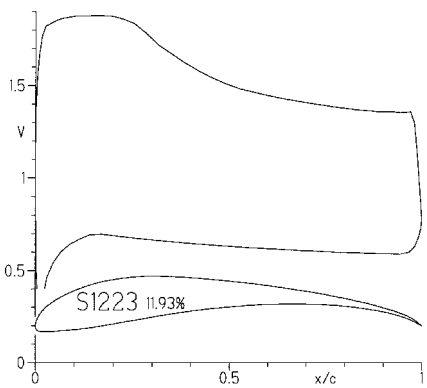

Fig. 13 Inviscid velocity distribution for the S1223 airfoil at $C_l = 1.95$.

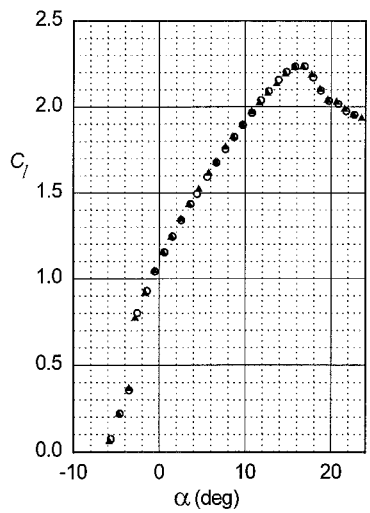

Fig. 14 Lift characteristics for the S1223 airfoil at $Re = 2 \times 10^5$.

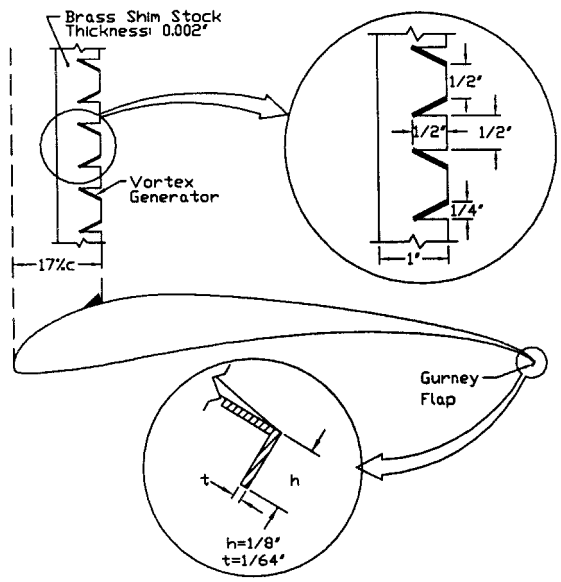

Fig. 15 Vortex generators and Gurney flap geometries used separately on the S1223 airfoil.

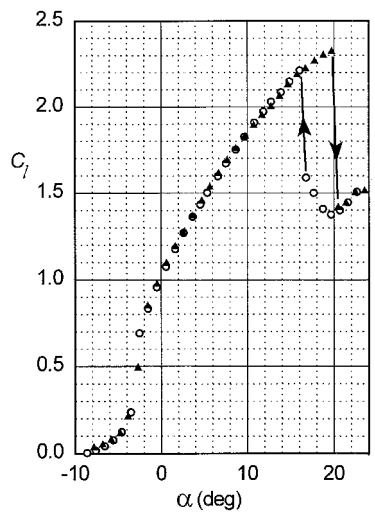

Fig. 16 Lift characteristics for the S1223 airfoil with vortex generators at $Re = 2 \times 10^5$.

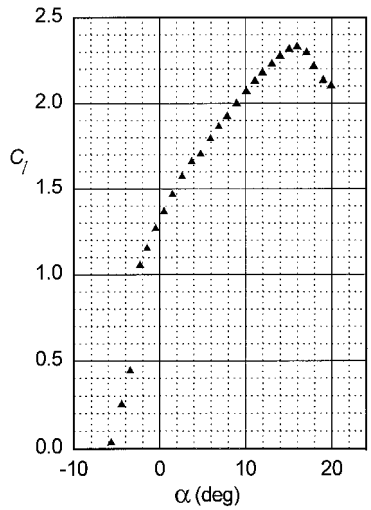

Fig. 17 Lift characteristics for the S1223 airfoil with a 1% chord Gurney flap at $Re = 2 \times 10^5$.

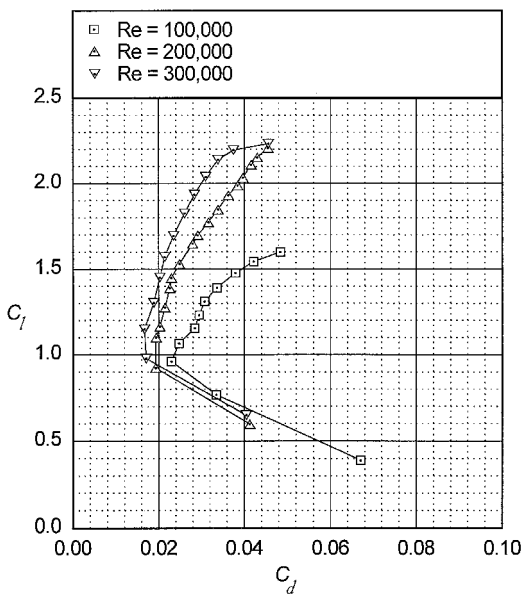

Fig. 18 Drag polar for the S1223 airfoil.

further data were taken since the airfoil was partially stalled, in which case the accuracy of the wake rake measurements are suspect.[22] As compared with the FX 63-137, the S1223 has higher drag, which must be expected for such high maximum lift coefficients.

VI. Conclusions

As a result of this work, it is clear that low Reynolds number airfoils can be designed to achieve lift coefficients much higher than previously thought possible. Such high-lift performance can be achieved through the use of a design philosophy that fully exploits the favorable effects of both a concave pressure recovery and aft loading. Application of this philosophy was demonstrated through the successful design of an airfoil that achieved a $C_{l,\max} = 2.2$ at a $Re = 2 \times 10^5$. Surprisingly, as the example airfoil illustrates, the pressure recovery for this class of airfoils, though concave and close to a Stratford distribution, can be tailored to produce acceptable stall characteristics for UAV applications.

Acknowledgments

This work was funded through private donations to the University of Illinois at Urbana–Champaign in support of a program to test low Reynolds number airfoils. The help of Philippe Giguére and Andy P. Broeren during the wind-tunnel tests is gratefully acknowledged. Finally, the meticulous efforts of Mark Allen (builder of the M06-12-138 and FX 63-137 wind-tunnel models), Jerry Robertson (E387), and Yvan Tinel (S1223) are greatly appreciated.

References

[1]Wortmann, F. X., "The Quest for High Lift," *Proceedings of the AIAA/MIT/SSA 2nd International Symposium of the Technology and Science of Low-Speed and Motorless Flight*, Soaring Society of America, Los Angeles, CA, 1974, pp. 97–101; also AIAA Paper 74-1018, Sept. 1974.

[2]Liebeck, R. H., and Ormsbee, A. I., "Optimization of Airfoils for Maximum Lift," *Journal of Aircraft*, Vol. 7, No. 5, 1970, pp. 409–415.

[3]Miley, S. J., "On the Design of Airfoils for Low Reynolds Numbers," *Proceedings of the AIAA/MIT/SSA 2nd International Symposium of the Technology and Science of Low-Speed and Motorless Flight*, Soaring Society of America, Los Angeles, CA, 1974, pp. 82–96; also AIAA Paper 74-1017, Sept. 1974.

[4]Eppler, R., *Airfoil Design and Data*, Springer–Verlag, New York, 1990.

[5]Foch, J. R., and Toot, P. L., "Flight Testing Navy Low Reynolds Number (LRN) Unmanned Aircraft," *Lecture Notes in Engineering: Low Reynolds Number Aerodynamics*, edited by T. J. Mueller, Vol. 54, Springer–Verlag, New York, 1989, pp. 407–417.

[6]Foch, J. R., and Ailinger, K. G., "Low Reynolds Number, Long Endurance Aircraft Design," AIAA Paper 92-1263, Feb. 1992.

[7]Bovais, C., and Toot, P., "Flight Testing the Flying Radar Target (FLYRT)," AIAA Paper 94-2144, June 1994.

[8]Karch, L. G., "Very Low Cost UAVs: Why We Need Them, What More We Need to Do," *Marine Corps Gazette*, March 1991, pp. 54–57.

[9]Liebeck, R. H., "Low Reynolds Number Airfoil Design at the Douglas Aircraft Company," *Proceedings of the Aerodynamics at Low Reynolds Numbers $10^4 < Re < 10^6$ International Conference*, Vol. 1, The Royal Aeronautical Society, London, 1986, pp. 7.1–7.24.

[10]Liebeck, R. H., "Design of Subsonic Airfoils for High Lift," *Journal Aircraft*, Vol. 15, No. 9, 1978, pp. 547–561.

[11]Van Ingen, J. L., and Boermans, L. M. M., "Aerodynamics at Low Reynolds Numbers: A Review of Theoretical and Experimental Research at Delft University of Technology," *Proceedings of the Aerodynamics at Low Reynolds Numbers $10^4 < Re < 10^6$ International Conference*, Vol. 1, The Royal Aeronautical Society, London, 1986, pp. 1.1–1.40.

[12]Maughmer, M. D., and Somers, D. M., "Design and Experimental Results for a High-Altitude, Long-Endurance Airfoil," *Journal of Aircraft*, Vol. 26, No. 2, 1989, pp. 148–153.

[13]Althaus, D., and Wortmann, F. X., *Stuttgarter Profilkatalog I*, Vieweg, Brunswick, Germany, 1981, ISBN 3-528-08464-2.

[14]Althaus, D., *Profilpolaren für den Modellflug*, Neckar–Verlag, Villingen-Schwenningen, Germany, 1980.

[15]Althaus, D., *Profilpolaren für den Modellflug*, Vol. 2, Neckar–Verlag, Villingen-Schwenningen, Germany, 1985.

[16]Mueller, T. J., "Low Reynolds Number Vehicles," AGARDograph 288, Feb. 1985.

[17]Guglielmo, J. J., and Selig, M. S., "Spanwise Variations in Profile Drag for Airfoils at Low Reynolds Numbers," *Journal of Aircraft*, Vol. 33, No. 4, 1996, pp. 699–707.

[18]Guglielmo, J. J., "Spanwise Variations in Profile Drag for Airfoils at Low Reynolds Numbers," M.S. Thesis, Dept. of Aeronautical and Astronautical Engineering, Univ. of Illinois at Urbana–Champaign, IL, 1995.

[19]Selig, M. S., Guglielmo, J. J., Broeren, A. P., and Giguére, P., *Summary of Low-Speed Airfoil Data*, Vol. 1, SoarTech Publications, Virginia Beach, VA, 1995.

[20]Selig, M. S., Lyon, C. A., Giguére, P., Ninham, C. P., and Guglielmo, J. J., *Summary of Low-Speed Airfoil Data*, Vol. 2, SoarTech Publications, Virginia Beach, VA, 1996.

[21]Giguére, P., and Selig, M. S., "Freestream Velocity Measurements and Corrections for Two-Dimensional Testing with Splitter Plates," AIAA Paper 96-2388, June 1996.

[22]Rae, W. H., Jr., and Pope, A., *Low-Speed Wind Tunnel Testing*, Wiley, New York, 1984.

[23]McGhee, R. J., Walker, B. S., and Millard, B. F., "Experimental Results for the Eppler 387 Airfoil at Low Reynolds Numbers in the Langley Low-Turbulence Pressure Tunnel," NASA TM-4062, Oct.

1988.
[24]Coleman, H. W., and Steele, W. G., Jr., *Experimentation and Uncertainty Analysis for Engineers*, Wiley, New York, 1989.
[25]Selig, M. S., Lyon, C. A., and Broeren, A. P., "Boundary Layer Turbulators on Airfoils at Low Reynolds Numbers," AIAA Paper 97-0511, Jan. 1997.
[26]Volkers, D. F., "Preliminary Results of Wind Tunnel Measurements on Some Airfoil Sections at Reynolds Numbers Between 0.6 $\times$ 10^5 and 5.0 $\times$ 10^5," Delft Univ. of Technology, Memo M-276, Delft, The Netherlands, 1977.
[27]Althaus, D., "Recent Wind Tunnel Experiments at Low Reynolds Numbers," *Proceedings of the Aerodynamics at Low Reynolds Numbers* $10^4 < Re < 10^6$ *International Conference*, Vol. 2, The Royal Aeronautical Society, London, 1986, pp. 18.1–18.42.
[28]Selig, M. S., and Guglielmo, J. J., "High-Lift Low Reynolds Number Airfoil Design," AIAA Paper 94-1866, June 1994.
[29]Selig, M. S., and Maughmer, M. D., "A Multipoint Inverse Airfoil Design Method Based on Conformal Mapping," *AIAA Journal*, Vol. 30, No. 5, 1992, pp. 1162–1170.
[30]Selig, M. S., and Maughmer, M. D., "Generalized Multipoint Inverse Airfoil Design," *AIAA Journal*, Vol. 30, No. 11, 1992, pp. 2618–2625.
[31]Selig, M. S., "Multipoint Inverse Design of Isolated Airfoils and Airfoils in Cascade in Incompressible Flow," Ph.D. Dissertation, Dept. of Aerospace Engineering, Pennsylvania State Univ., University Park, PA, May 1992.
[32]Eppler, R., and Somers, D. M., "A Computer Program for the Design and Analysis of Low-Speed Airfoils," NASA TM-80210, Aug. 1980.
[33]Drela, M., and Giles, M. B., "Viscous-Inviscid Analysis of Transonic and Low Reynolds Number Airfoils," *Journal of Aircraft*, Vol. 25, No. 10, 1987, pp. 1347–1355.
[34]Somers, D. M., "Subsonic Natural-Laminar-Flow Airfoils," *Natural Laminar Flow and Laminar Flow Control*, edited by R. W. Barnwell and M. Y. Hussaini, Springer–Verlag, New York, 1992, pp. 143–176.
[35]Eppler, R., *Laminar Airfoils for Reynolds Numbers Greater than* 4×10^6, National Technical Information Service, N69-28178, translated from Ingenieur-Archiv, Bd. 38, Heft 4/5, B-819-35, April 1969, pp. 232–240.

S1223

1.00000	0.00000
0.99838	0.00126
0.99417	0.00494
0.98825	0.01037
0.98075	0.01646
0.97111	0.02250
0.95884	0.02853
0.94389	0.03476
0.92639	0.04116
0.90641	0.04768
0.88406	0.05427
0.85947	0.06089
0.83277	0.06749
0.80412	0.07402
0.77369	0.08044
0.74166	0.08671
0.70823	0.09277
0.67360	0.09859
0.63798	0.10412
0.60158	0.10935
0.56465	0.11425
0.52744	0.11881
0.49025	0.12303
0.45340	0.12683
0.41721	0.13011
0.38193	0.13271
0.34777	0.13447
0.31488	0.13526
0.28347	0.13505
0.25370	0.13346
0.22541	0.13037
0.19846	0.12594
0.17286	0.12026
0.14863	0.11355
0.12591	0.10598
0.10482	0.09770
0.08545	0.08879
0.06789	0.07940
0.05223	0.06965
0.03855	0.05968
0.02694	0.04966
0.01755	0.03961
0.01028	0.02954
0.00495	0.01969
0.00155	0.01033
0.00005	0.00178
0.00044	-0.00561
0.00264	-0.01120
0.00789	-0.01427
0.01718	-0.01550
0.03006	-0.01584
0.04627	-0.01532

0.06561	-0.01404
0.08787	-0.01202
0.11282	-0.00925
0.14020	-0.00563
0.17006	-0.00075
0.20278	0.00535
0.23840	0.01213
0.27673	0.01928
0.31750	0.02652
0.36044	0.03358
0.40519	0.04021
0.45139	0.04618
0.49860	0.05129
0.54639	0.05534
0.59428	0.05820
0.64176	0.05976
0.68832	0.05994
0.73344	0.05872
0.77660	0.05612
0.81729	0.05219
0.85500	0.04706
0.88928	0.04088
0.91966	0.03387
0.94573	0.02624
0.96693	0.01822
0.98255	0.01060
0.99268	0.00468
0.99825	0.00115
1.00000	0.00000